ELSEVIER

Journal of Fluids and Structures 20 (2005) 913–925

JOURNAL OF FLUIDS AND STRUCTURES

www.elsevier.com/locate/jfs

Instability of a long ribbon hanging in axial air flow

C. Lemaitre, P. Hémon, E. de Langre*

Département de Mécanique, LadHyX, Ecole Polytechnique, 91128 Palaiseau, France

Received 20 April 2004; accepted 9 April 2005

Abstract

A ribbon hanging in a vertical air stream experiences sudden vibrations by flutter when the flow velocity reaches a critical value. The experiments conducted here for strips made of different materials show two distinct behaviours depending on the length of the strip. For short strips, the critical flow velocity depends strongly on the length, whereas for longer strips the critical velocity becomes independent of the length. These behaviours are analysed using a model originally derived by Datta, based on a slender-body approximation and unsteady potential flow theory. This yields an equation of motion similar to that pertaining to a hanging pipe-conveying fluid. The corresponding critical velocities are in relatively good agreement with those of the experiments for a set of 12 different ribbons. An asymptotic critical velocity may thus be defined corresponding to the limit of very long ribbons. The model predicts that this velocity only depends on the ratio between the fluid added mass and the ribbon mass. This is compared with experiments using strips of various widths and materials, and relation is made to the case of a hanging fluid-conveying pipe, addressed in a recent paper, and with the case of long towed cylinders.

Keywords: Flutter; Ribbon; Axial flow

1. Introduction

Vibration of flexible membranes and plates due to axial air-flow is an important issue, for instance, in paper manufacturing and paper printing (Watanabe et al., 2002a). In those industries, long bands of paper are fed through machines at high speed. Paper is consequently swept by an air-flow which is likely to cause oscillatory instabilities. Such vibrations can provoke folding, wrinkling and even tearing of the paper bands, thereby limiting the production pace. The onset of such instabilities depends on the flow velocity, the tension of the paper as well as its material and geometric characteristics.

An important parameter in the physics of this phenomenon is the ratio between the length, L, and the width, B, of the flexible structure, Fig. 1. Typical values of this ratio in the literature are given in Table 1. Limit values of the aspect ratio L/B are associated with quite different phenomena and models. The case of small aspect ratios, say $L/B<1$, corresponds to flags or sheets and also to the particular case of filaments in a flowing soap film, as in Zhang et al. (2000) and Farnell et al. (2004a,b). Experiments in that range may be found, for instance, in Watanabe et al. (2002a), Huang (1995) and Yamaguchi et al. (2000). Theoretical approaches, see Païdoussis (2003) for a review, have shown that these

*Corresponding author. Tel.: +33 1 69 33 36 01; fax: +33 1 69 33 30 30.
E-mail address: delangre@ladhyx.polytechnique.fr (E. de Langre).

0889-9746/$ - see front matter © 2005 Elsevier Ltd. All rights reserved.
doi:10.1016/j.jfluidstructs.2005.04.009

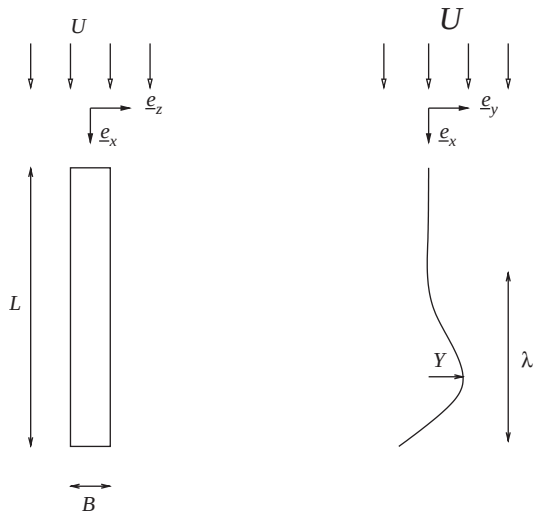

Fig. 1. Geometrical parameters of a ribbon subjected to axial flow.

Table 1
Aspect ratio and dominant tensioning effect in experiments

	L/B	Tensioning effect	Comment
Zhang et al. (2000)	0	Friction	Filament in soap film
Watanabe et al. (2002a)	0.25–1.4	Friction	
Huang (1995)	0.67–1.7	Friction	
Yamaguchi et al. (2000)	1.2–12	Friction	
Datta and Gottenberg (1975)	4–22	Gravity	
Bejan (1982)	10–16	Friction	Falling ribbon
Present paper	4–50	Gravity	

cases may be approximated by considering a 2-D approximation in the (x, y) plane, Fig. 1. Conversely, large aspect ratios correspond to strips or ribbons. Experiments by Datta and Gottenberg (1975) and Bejan (1982) fall in that range. For these geometries a slender-body approximation is more appropriate, where the fluctuating velocities resulting from the deformation are mainly in the (y, z) plane, transverse to the axis of the ribbon. This yields models similar to those pertaining to other slender bodies in axial flow, such as cylinders. Note that for such slender ribbon, experiments are usually done with flow in the vertical direction, as gravity would not allow horizontal strips to have a straight initial position. The consequences in terms of the main tensioning effect, friction for horizontal structures and gravity for vertical ones, will be discussed further.

In this paper our purpose is to explore the case of large aspect ratios only. It should be noted here that another aspect ratio may also be defined in terms of λ/B, where λ is the scale of variation of the deflection along the x-axis, Fig. 1. The slender-body approximation, which we shall use in this paper, is more precisely associated with the assumption that $\lambda \gg B$. In all cases considered here we shall have $L/B \gg 1$ and $\lambda/B \gg 1$.

A strip hanging in a vertical air-flow is observed to vibrate when the flow velocity is raised above a critical value, as shown by Datta and Gottenberg (1975) in experiments with Mylar strips. These authors also developed a model based on unsteady potential flow theory using the slender-body approximation mentioned above. In their computations the length of the hanging ribbon had a rather complex effect on the critical flow velocity that causes flutter: for short ribbons the critical velocity decreased with length whereas it was increasing with length for longer ribbons. Yadykin et al. (2001), in a computational approach of the same system, also found a decrease then an increase of the critical velocity for hanging ribbons of increasing length, for both linear and nonlinear approximations of the dynamics. On this particular issue of the effect of length, the experimental results of Datta and Gottenberg (1975) were not very conclusive, because of the scatter of data.

For other slender systems subjected to axial flow and with a downstream end free, such evolutions of the critical velocity, or more generally of the characteristics of the instability, have been reported. In those systems friction due to the flow is the cause of axial tension, in a manner somewhat equivalent to gravity in hanging systems. Ni and Hansen (1978) reported that in their experiment of water flow along a cable there exists an "active" length near the downstream end where most of the deformation occurs. For long cables they showed that this active length is more relevant than the true length to model the instability of the cable. They interpreted this effect by the attenuation of motion resulting from the increasing tension near the upstream end. Païdoussis (1966) noted that, in experiments on axial flow along cylinders, as the length is increased buckling disappears. Triantafyllou and Chryssostomidis (1984), considering only the divergence instabilities of a flexible cylinder with external flow found that the critical velocity becomes independent of length for very long cylinders. The case of a string (Triantafyllou and Chryssostomidis, 1985), though quite different in nature, or that of a filament (Schouveiler et al., 2004), also showed a strong influence of length. For axial flow along plates of various length-to-width ratios, also tensioned by friction, similar effects have been observed. Huang (1995) noted that for long plates under flow the motion is confined in a region close to the downstream end. Yamaguchi et al. (2000), and Watanabe et al. (2002b) defined several regimes in terms of the influence of length on the stability of plates in axial flow.

A parallel problem is that of a hanging pipe-conveying fluid, see Païdoussis (1998) for an extensive review. Recently, in Doaré and de Langre (2002), it was shown that an asymptotic régime does exist for long pipes, where the characteristics of the instabilities do not depend on the pipe length. This was found both in experiments and in computations using a standard model for the dynamics of the fluid-conveying pipe tensioned by gravity. The transition length between the two regimes could be simply derived by considering the local stability of bending waves.

The aim of the present paper is to conduct, for hanging ribbons under axial flow, an analysis similar to that of Doaré and de Langre (2002). In particular we seek to determine whether an asymptotic regime with constant critical velocity exists, as in pipes, or does not, as predicted by Datta and Gottenberg (1975) and Yadykin et al. (2001). In Section 2, new experimental results are given. They are analysed in Section 3 using the unsteady potential flow model of Datta and Gottenberg (1975). These results are discussed in Section 4.

2. Experiments

2.1. Experimental set-up

Tested ribbons are made of four different materials: paper, Mylar, fabric and silk. The paper is a classical printer paper, the fabric is from cotton sheets, the Mylar is a polyester film used as dielectrics, and the silk is taken from an advertising streamer. The flexural rigidity D of each ribbon is measured through the buckling height h_c which is the minimum height for which a vertical strip clamped at its bottom buckles under its own weight (Timoshenko, 1961)

$$D = \frac{h_c^3 mg}{7.83}, \tag{1}$$

where g denotes gravity and m is the mass per unit area.

Three different ribbon widths B are selected for each material: $B = 20, 30$, and $54\,\text{mm}$. Hence, a set of 12 different ribbons is investigated, and for each set several lengths are tested. The four materials have very different characteristics, as detailed in Table 2. The length of ribbons varies from $L = 0.2$ to $L = 1\,\text{m}$, so that the aspect ratio ranges approximately from $L/B = 4$ to $L/B = 50$. A given ribbon is hung in a vertical wind tunnel of diameter $d = 194\,\text{mm}$.

The Reynolds number is here $\text{Re} \simeq 5 \times 10^5$ based on $U = 4\,\text{m/s}$, a typical flow velocity, and the diameter of the test-section, so that the flow is fully turbulent. With a fine grid, a honeycomb and a convergent shape at the inlet, the experimental set-up provides a low turbulence level, of less than 0.1%, so that we may assume the flow conditions to be uniform and steady.

The flow velocity is progressively raised until the critical velocity U_c is reached where steady vibrations are observed in the (x, y) plane, Fig. 2. To analyse the dependence of U_c on L, we vary the length of the strip by progressively shortening it. About 300 values of critical flow velocities U_c are thus measured.

2.2. Experimental results

The critical flow velocity is plotted in Figs. 3 and 4 as a function of the ribbon length for each material and for each width. In all cases, two regimes may be observed. For short ribbons, the critical velocity depends strongly on the length,

Table 2
Characteristics of materials for the ribbons

	m (kg/m^2)	h_c (m)	D (Nm)	η (m)
Paper	0.0790	0.130	220×10^{-6}	0.065
Mylar	0.0516	0.072	24×10^{-6}	0.036
Fabric	0.2165	0.040	17×10^{-6}	0.020
Silk	0.0630	0.026	1.4×10^{-6}	0.013

m, mass per unit area; h_c, buckling height; D, flexural rigidity derived from Eq. (1); η, reference length.

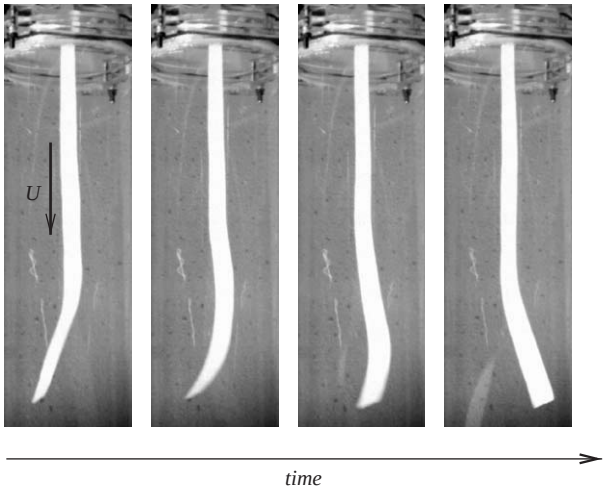

Fig. 2. Typical flutter motion of a hanging paper strip over a half-period.

whereas for long ribbons the critical velocity is weakly dependent on the length. This is more pronounced in the case of paper and Mylar, Fig. 3, than in the case of fabric and silk, Fig. 4. These evolutions are qualitatively similar to those observed for a fluid-conveying pipe (Doaré and de Langre, 2002).

3. Model

3.1. Unsteady potential flow model

Considering the aspect ratio L/B, as discussed in the first section, we use here a slender-body approximation whereby the fluctuating velocities are only in the (y, z) plane and an unsteady potential flow model to derive the fluid action, following Datta and Gottenberg (1975). The equation governing the lateral deflection of the strip then reads (Païdoussis, 2003)

$$D\frac{\partial^4 Y}{\partial X^4} - \frac{\partial}{\partial X}\left[(mg(L-X) - MU^2)\frac{\partial Y}{\partial X}\right] + 2MU\frac{\partial^2 Y}{\partial X \partial \tau} + (m+M)\frac{\partial^2 Y}{\partial \tau^2} = 0, \tag{2}$$

where Y is the deflection of the strip, τ is time, g is gravity, L is the total length of the strip, U is the flow velocity and M is the added mass due to the presence of the fluid. For a unit area of strip, the added mass which scales all fluid effects is taken as $M = \pi\rho B/4$. This models the added mass of an infinitely long rigid plate of width B in a transverse motion, where the added mass per unit length is $M_a = \pi\rho B^2/4$, leading to the value of $M = M_a/B$. Note that the added mass in air is not negligible here, being of the same order as the ribbon mass. In Eq. (2) the local fluid forces, which are scaled by the added mass M, are of three kinds: an added inertia force independent of U, a Coriolis type force proportional to U, and a stiffness force proportional to U^2.

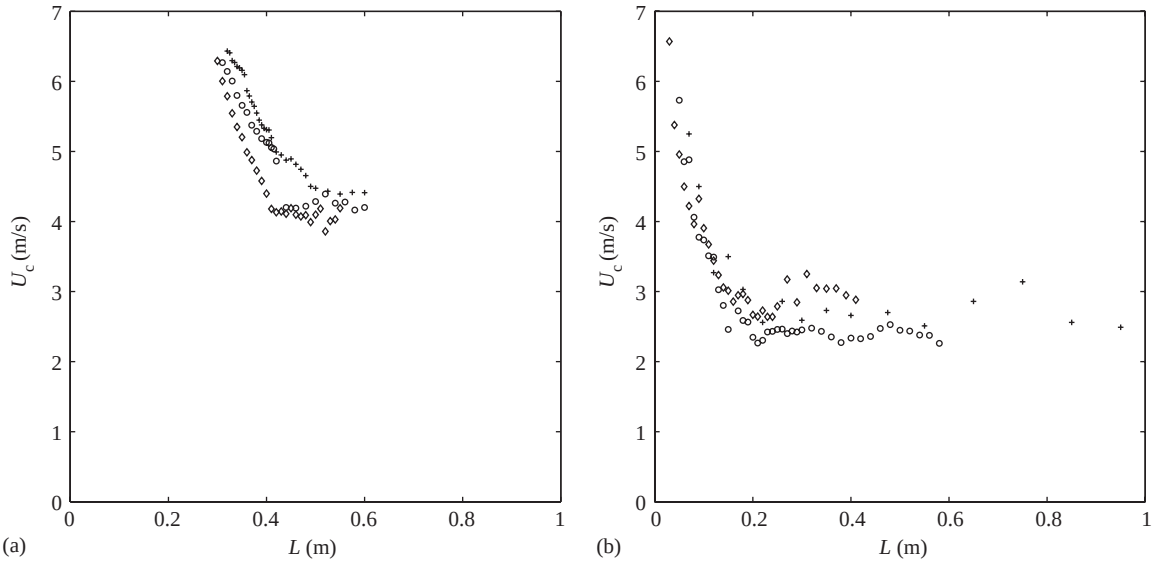

Fig. 3. Effect of the ribbon length on the critical velocity for flutter: (a) paper and (b) Mylar. Ribbon width: ◇, 20 mm; +, 30 mm; o, 55 mm.

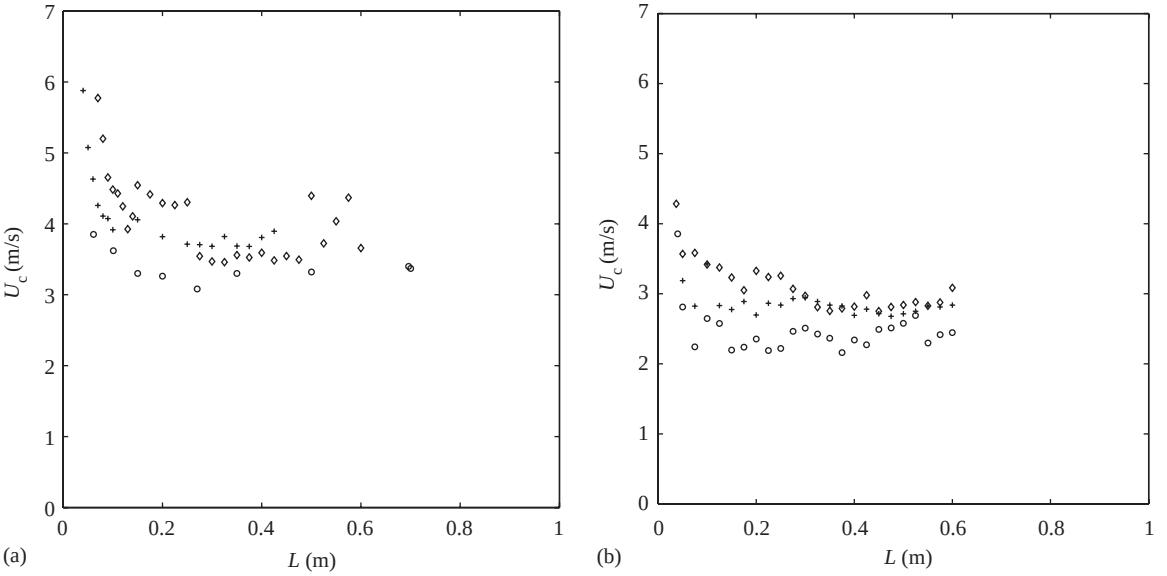

Fig. 4. Effect of ribbon length on the critical velocity for flutter: (a) fabric and (b) silk. Ribbon width: ◇, 20 mm; +, 30 mm; o, 55 mm.

Friction due to axial flow along the two sides of the ribbon have also been taken into account in the original model of Datta and Gottenberg (1975), through its additional tensioning effect, with the corresponding local tension

$$T(X) = mg(L - X) + f\rho U^{3/2} v^{1/2}(L^{1/2} - X^{1/2}), \tag{3}$$

where v is the viscosity of air and $f = 1.328$ is the laminar friction coefficient. Also, the dimensionless parameter F that scales tension due to friction and tension due to gravity at the upper end is

$$F = \frac{f\rho v^{1/2} U^{3/2}}{mgL^{1/2}}. \tag{4}$$

In all our experiments we have $F<0.05$. Hence, taking into account friction will have little influence on the predicted critical velocities. Another approximation on the role of friction for very long ribbons can be given as follows: close to the downstream end, a first-order expansion of $T(X)$ in Eq. (3) is $T(X)=mg(1+(F/2))(L-X)$. This yields an apparent increase of the tension due to gravity by a factor of $(1+F/2)$ only. Clearly, for $F<0.05$, friction does not play any role in our experiments and we shall neglect it from now on.

The boundary conditions associated to Eq. (2) are

$$Y(0)=\frac{\partial Y}{\partial X}(0)=0, \quad \frac{\partial^2 Y}{\partial X^2}(L)=\frac{\partial^3 Y}{\partial X^3}(L)=0, \tag{5}$$

respectively, for the clamped top and for the free extremity at the bottom. The boundary condition at the downstream end, in a slender body approximation, takes the form of conditions on the shear force and bending moment. The condition used here in Eq. (5) implies that no particular lift is generated there. A full discussion on the effect of other choices of boundary conditions may be found in Païdoussis (2003) in the parallel case of cylinders with various end shapes.

In order to now define dimensionless variables we use as reference the length

$$\eta=(D/mg)^{1/3} \tag{6}$$

instead of the length of the ribbon, following Doaré and de Langre (2002). This is necessary as we seek to vary the length L itself. This new length η results from the relative magnitudes of the flexural rigidity and stiffness due to tension induced by gravity. Here η is of a few centimeters, see Table 2. Combining Eqs. (1) and (6) yields $\eta \simeq h_c/1.98$. We now define

$$x=\frac{X}{\eta}, \quad y=\frac{Y}{\eta}, \quad t=\left[\frac{mg}{\eta(M+m)}\right]^{1/2}\tau, \quad v=\left[\frac{M}{\eta mg}\right]^{1/2}U, \quad \beta=\frac{M}{M+m}, \quad \ell=\frac{L}{\eta}. \tag{7}$$

Eq. (2) then becomes

$$\frac{\partial^4 y}{\partial x^4}-\frac{\partial}{\partial x}\left[(\ell-x)\frac{\partial y}{\partial x}\right]+v^2\frac{\partial^2 y}{\partial x^2}+2\sqrt{\beta}v\frac{\partial^2 y}{\partial x \partial t}+\frac{\partial^2 y}{\partial t^2}=0 \tag{8}$$

with clamped boundary conditions, $y'(0)=y''(0)=0$ at the top end and free conditions at the bottom end, $y''(\ell)=y'''(\ell)=0$. This equation is identical to the one used by Doaré and de Langre (2002) for long hanging fluid-conveying pipes. Note that, for typical values of the parameters in our experiments, the dimensionless velocity v is of order 1, so that both velocity-dependent terms in Eq. (8) are of similar order of magnitude, and none of them can be neglected.

The dimensionless mass ratio, β, depends on the characteristics of the material of the ribbon but also on its width,

$$\beta=\frac{(\rho\pi B/4)}{(\rho\pi B/4)+m}=\frac{(\rho\pi B^2/4)}{(\rho\pi B^2/4)+mB}. \tag{9}$$

This originates from the added mass per unit length varying as B^2 whereas the ribbon mass varies as B. Table 3 gives the range of mass ratio in our experiments. These values show that added mass, though the fluid is air, is not negligible here.

3.2. Critical velocity

At a given dimensionless flow velocity v, the strip is unstable if one of the eigenmodes of this system has a negative damping. The critical velocity v_c is the lowest value of v such that an unstable mode exists. The governing dimensionless parameters are the reduced ribbon length ℓ, the flow velocity v and the mass ratio β. The critical velocity v_c therefore depends on two parameters, ℓ and β. We derive now the characteristics of the eigenmodes under flow, and thus the critical velocity, using a Galerkin approximation based on the eigenmodes without flow or gravity, as in Doaré and de Langre (2002). We use up to 50 modes in our computations. This is done for the 12 different values of β, Table 3, as a function of the dimensionless length ℓ.

In Figs. 5 and 6, we compare results of the model with experimental data on four typical cases. The dependence of the critical velocity with length is qualitatively similar to that observed in the experiments: (a) for short ribbons the dependence is strong, (b) for long ribbons the dependence is weak. In Doaré and de Langre (2002), the length where transition between these two regimes occurs in a hanging pipe was found to be well approximated in dimensionless form by $\ell=4$. In Figs. 5 and 6, this appears to be also a reasonable approximation of the transition between the two regimes,

Table 3
Mass ratio depending on the material and the ribbon width

Material	Width B (mm)	Mass ratio β
Paper	20	0.19
	30	0.26
	54	0.40
Mylar	20	0.27
	30	0.35
	54	0.50
Fabric	20	0.08
	30	0.12
	54	0.19
Silk	20	0.23
	30	0.31
	54	0.45

in the computation and in the experiments. Quantitative prediction of the critical velocity for long ribbons, as for short ribbons is found to be much more accurate for the experiments with Mylar. This will be discussed in the last section.

3.3. The long ribbon limit

Both the experiments and the model show a small dependence on length of the critical velocity for long ribbons. We may therefore define for each ribbon an asymptotic critical velocity, v_c^∞, by simply considering the minimum value of the critical velocity v for all values of ℓ. In the model this velocity only depends on the mass ratio β. We now compare in Fig. 7 the experimental values of this asymptotic velocity with those derived from the model, for all values of β given in Table 3.

Several conclusions may be drawn from this comparison.

(a) Qualitatively, the order of magnitude of v_c^∞ and its scale of dependence with the mass ratio β is recovered. Note that comparison of more refined models with similar experiments (Yadykin et al., 2001; Watanabe et al., 2002b; Yamaguchi et al., 2000) show quantitative discrepancies of the same order of magnitude.

(b) For all materials, the experimental results of thin ribbons ($B = 20$ mm) are better approximated than those for wide ribbons ($B = 54$ mm). This may be understood by considering that the slender-body approximation is more applicable for thin ribbons which have a larger aspect ratio. Moreover, the effect of the finite width of the wind-tunnel would have more influence on the wider strips.

(c) Results for Mylar and paper are more accurately predicted than for fabric and silk. As these differences in behaviour also appear in the critical velocity for ribbons of short length, it is believed that they result from the behaviour of the material itself, modelled here as purely elastic. The addition of internal damping in the model is discussed further in Section 3.4.

(d) Nonlinear effects may also play a role, as the critical velocity is determined experimentally from the existence of a limit-cycle oscillation. Yet, Yadykin et al. (2001) showed that for this problem nonlinear effects would lead to a lower critical velocity than that predicted by the linear theory (subcritical case). Hence, nonlinear effects are not responsible for the quantitative differences observed here.

3.4. Effect of damping

The results of Fig. 7 suggest that a mechanism depending on the material of the ribbons should be taken into account to improve the model. We investigate here the influence of material damping, as the materials used in experiments have very different internal structures: Mylar has a crystal-like structure, whereas the others are made of fibers, more or less organised. Paper fibres hold tightly together compared to fabric and silk which are loosely woven. Following Païdoussis (1998), the material damping is modelled by adding a new term in the dimensionless equation, leading to

$$\sigma \frac{\partial^5 y}{\partial t \partial x^4} + \frac{\partial^4 y}{\partial x^4} - \frac{\partial}{\partial x}\left[(\ell - x)\frac{\partial y}{\partial x}\right] + v^2 \frac{\partial^2 y}{\partial x^2} + 2\sqrt{\beta} v \frac{\partial^2 y}{\partial x \partial t} + \frac{\partial^2 y}{\partial t^2} = 0, \tag{10}$$

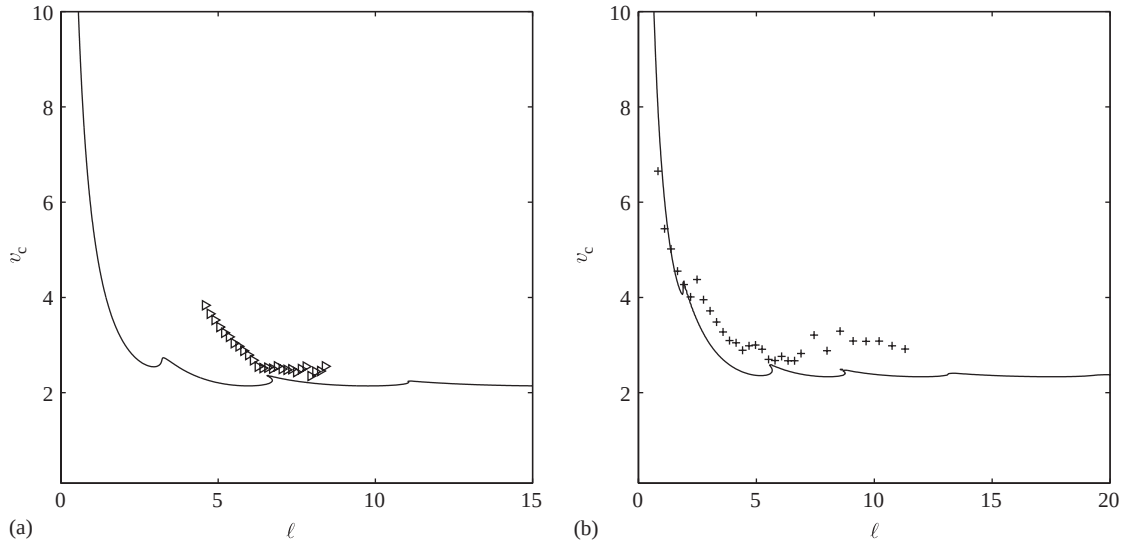

Fig. 5. Effect of the dimensionless ribbon length on the dimensionless critical velocity: —, computations; ▷, +, experiments. (a) Paper, $B = 20\,\text{mm}$; (b) Mylar, $B = 20\,\text{mm}$.

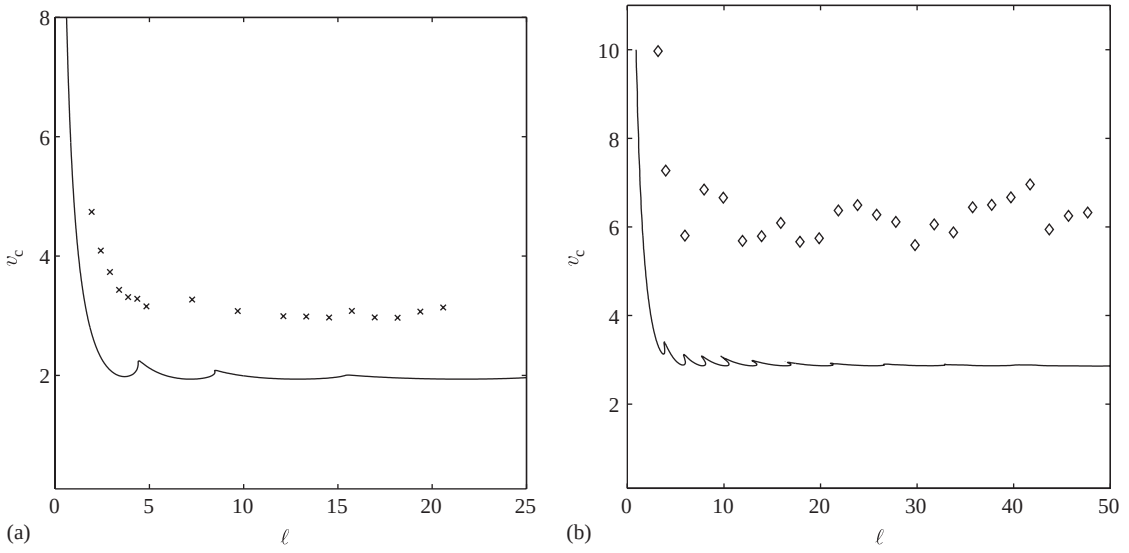

Fig. 6. Effect of the dimensionless ribbon length on the dimensionless critical velocity: —, computations; ×, ◇, experiments. (a) Fabric, $B = 30\,\text{mm}$; (b) silk, $B = 55\,\text{mm}$.

where σ is the dimensionless internal damping,

$$\sigma = \frac{D'(mg)^{2/3}}{D^{7/6}(m+M)^{1/2}}, \tag{11}$$

D' being the internal damping coefficient. This internal damping models dissipative effects that are proportional to the variation of local strain with time, as opposed to those proportional to velocities. The former are typically used to model dissipative effects that take place in the structure of the material, the latter for effects related to the interaction with the external media such as added fluid damping for instance. Note that here all dimensionless variables are built with a reference length, Eq. (6), which is not that of the ribbon but results from the relative magnitudes of the flexural

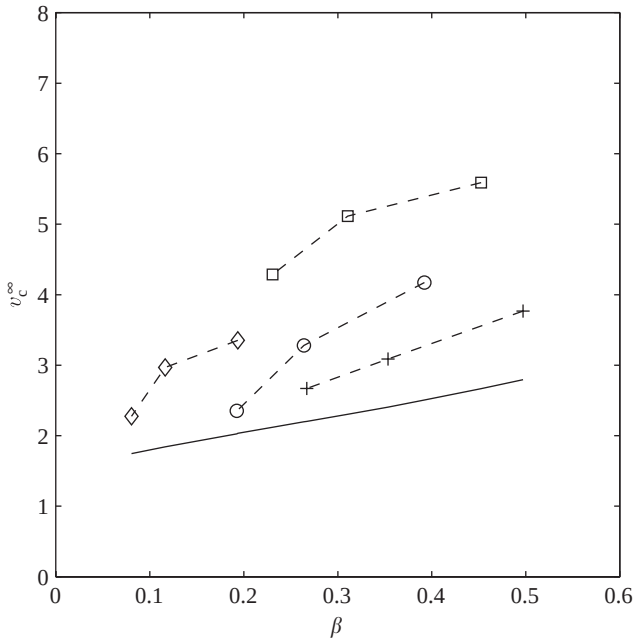

Fig. 7. Dependence of the asymptotic critical velocity with the mass ratio: —, Model, Eq. (8); □, silk; o, paper; +, Mylar; ⋄, fabric.

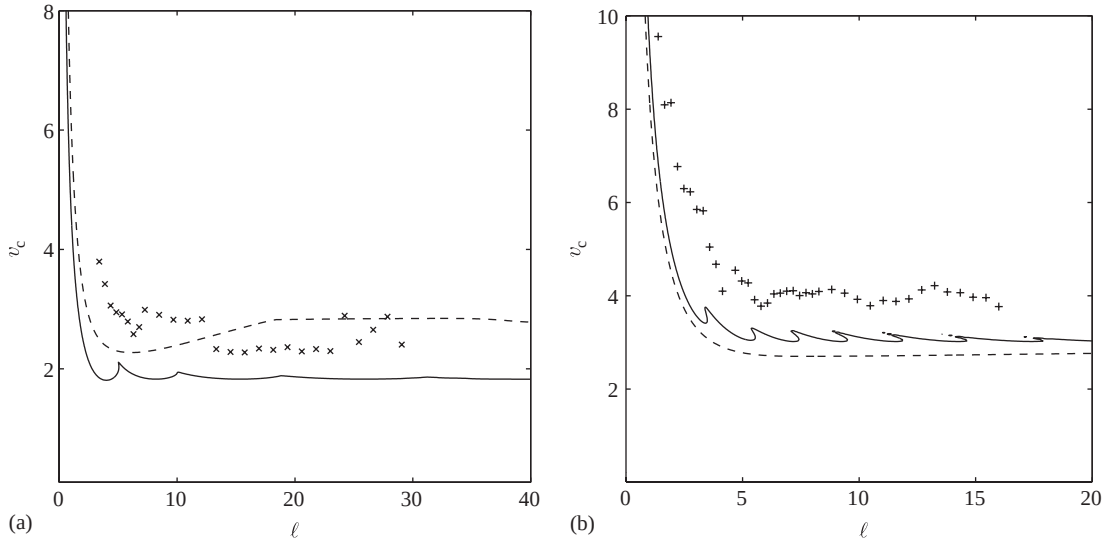

Fig. 8. Effect of the material damping on the critical velocity: —, computation without damping; - - -, computation with damping $\alpha = 0.1$; ×, +, experiments. (a) Fabric, $B = 20\,\text{mm}$, $\beta = 0.08$; (b) Mylar, $B = 54\,\text{mm}$, $\beta = 0.50$.

rigidity and stiffness due to gravity. Therefore, as the length of the ribbon is varied, the dimensionless internal damping α defined in Païdoussis (1998) varies as $\alpha = \sigma/\ell^2$. From simple free oscillation experiments, using a procedure similar to that of Païdoussis (1998) we found the order of magnitude of α to be 0.1. In Fig. 8, results of the model with damping are shown. In Fig. 8(a), where $\beta = 0.08$, the computed critical velocities are higher with damping than without. In Fig. 8(b), where $\beta = 0.50$, damping leads to lower values of v_c, indicating destabilisation. The destabilisation effect of damping at high mass ratios β in Eq. (10) is a well known feature for short length systems Païdoussis (1998). We may

conclude that material damping, whatever its true value, cannot be the source of all differences between the model and the experiments, particularly at high mass ratios.

4. Discussion

4.1. On the mechanism of flutter

Using the model of Eq. (8), the mechanism of flutter is identical to that of fluid-conveying pipes, as the equation of motion is identical. A detailed description of this may be found in Païdoussis (1998), but some elements need to be recalled for the discussion on the effect of length. In the limit of small mass ratios, $\beta \ll 1$, the instability arises by coupled-mode flutter between two modes of comparable wavelength. The fluid force responsible for this is the stiffness term, proportional to v^2 in Eq. (8), that simultaneously modifies the frequencies of the modes, allowing coalescence of the frequencies, and produces a nonsymmetric coupling between the two modes. In our case of flow along a ribbon, this stiffness force induced by the flow is simply the consequence of the local curvature of the ribbon surface on the local dynamic pressure [see Païdoussis (2003) for a more general discussion on the relation between inviscid terms in models for external axial flow on slender structures and in models for internal axial flow]. Note that the limit case of $\beta = 0$ is identical to that of dynamic instability of a beam subjected to a compressive follower force (Bolotin, 1963). For increasing values of the mass ratio β, the pure coupled-mode flutter is progressively modified, flutter arising by a continuous evolution of the characteristics of one of the modes, without coalescence of the frequencies.

4.2. On the numerical method

The Galerkin method used here is a straightforward extension of that used for various problems of fluid-conveying pipes in Païdoussis (1998) or ribbons in axial flow (Datta and Gottenberg, 1975). It is identical to that used by Doaré and de Langre (2002) to analyse the effect of length on the stability of fluid-conveying pipes. The modes used in the Galerkin expansion are those of a cantilevered beam, without tension induced by gravity nor flow effects. A typical convergence of the results is shown in Fig. 9(a), where the critical velocity for a long ribbon is shown to become independent of the number of modes for more that 15 modes approximately in that case. Fig. 9(b) shows that whereas the use of 5 modes only would give a good approximation for the critical velocity of a short ribbon, say $\ell < 5$, it yields erroneous results for longer ribbons.

Indeed, only a small number of modes is needed to compute the critical velocity for short systems, as the instability results then from the combination of the first modes only. Païdoussis (1998) discusses a similar point on the number of modes needed to properly predict the instability threshold of fluid-conveying pipes, depending on the mass ratio β. He showed that the loops in the critical velocity curve were related to the increase in the (small) number of modes playing a role in the instability. Here, similar loops can be observed in the numerical predictions of the critical velocity when the length is varied, so that an increase of the number of modes playing a role in the instability may be expected. In fact, we observed, both in experiments and in computation, that for long systems the part of the ribbon that moves in the instability is confined to the lower part, that its extent is nearly independent of length, as well as the apparent wavelength. We interpret this as the instability resulting from the combination of modes that have mode shapes with about that constant wavelength: these modes having higher and higher ranks as the length is increased, more and more modes are needed to accurately predict the critical velocity. If the number of modes used is not sufficient, an erroneous increase of the critical velocity with length is found. This is parallel to the erroneous prediction of the critical velocity at high mass ratio for short pipes, as discussed in Païdoussis (1998).

A typical mode shape near the instability threshold for a long ribbon, Fig. 10, shows that the set of modes used allow to describe a motion similar to that observed in the experiments, Fig. 2.

4.3. On the effect of length

The experimental and numerical results presented here show that there exists a length above which the critical velocity for flutter of hanging ribbons in axial flow becomes approximately independent of length. In the experiments this appears for all ribbons tested. Earlier experimental results by Datta and Gottenberg (1975) did not allow to demonstrate this long ribbon regime, because of the scatter of experimental data. The present experiments, with several materials and several aspect ratios, cover a much larger parameter space than that of Datta and Gottenberg (1975).

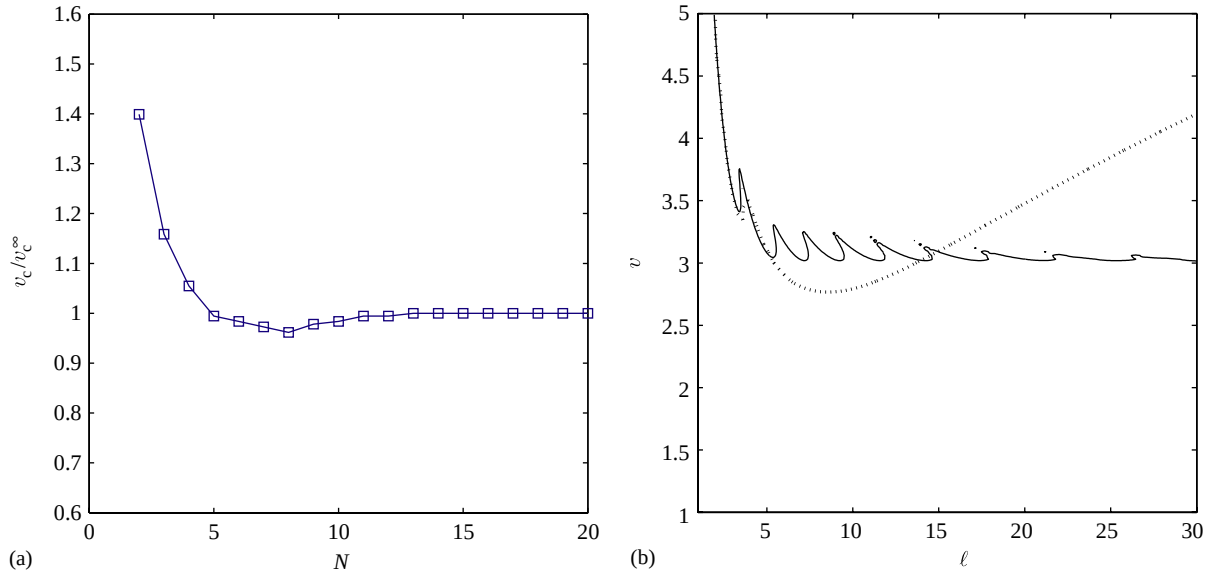

Fig. 9. Effect of the number of modes used in the Galerkin approximation on the computed critical velocity v. (a) Evolution of the ratio v_c/v_c^∞ with the number of modes N, for $\ell = 15$, $\beta = 0.08$. (b) Evolution of the critical velocity with length using 5 modes (...) or 50 modes (—), for $\beta = 0.5$.

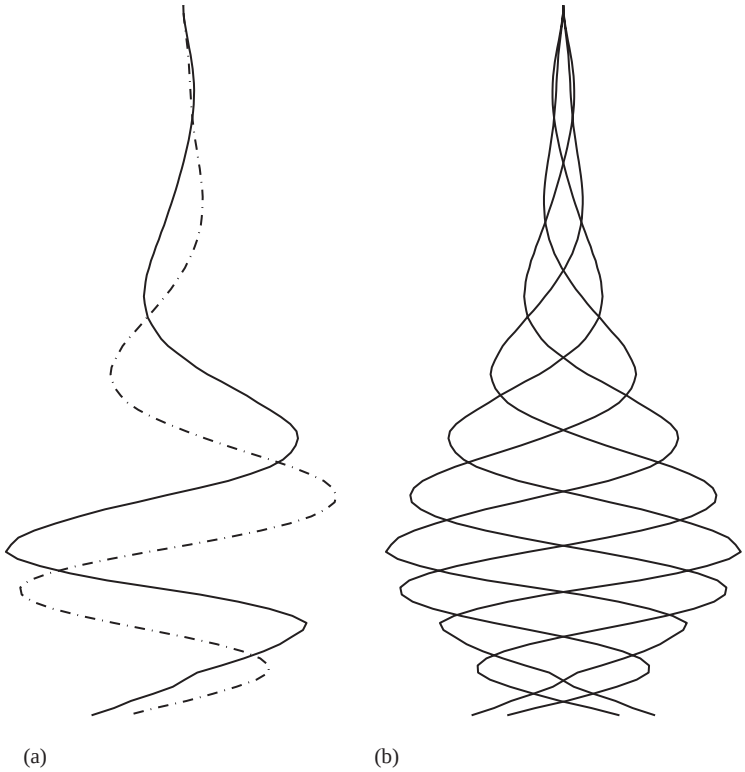

Fig. 10. Computed mode shape at instability for $\beta = 0.26$, $\ell = 15$, $v = 3$. (a) Real (—) and imaginary (- · -) part of the mode shape. (b) Deformation at four instants of the cycle of oscillation.

Our numerical results are also consistent with those obtained by Doaré and de Langre (2002) for hanging fluid-conveying pipes, who evidenced a long pipe regime. We have shown that the equation proposed in Datta and Gottenberg (1975) may be put in a dimensionless form identical to that used by Doaré and de Langre (2002). Using the same equation but with terms accounting for axial friction of the flow, Datta and Gottenberg (1975) and more recently Yadykin et al. (2001) found that the critical velocity should increase with length for very long systems, in contradiction with our finding. Friction is not the reason for the difference between our results and theirs, as we have shown here that frictional force effects play a negligible role in this range of parameters, in comparison with gravity. The difference may be explained by considering that in their Galerkin computations these authors used a much smaller number of modes: 3 in Datta and Gottenberg (1975) and 8 in Yadykin et al. (2001), while we used up to 50 in our computations. The convergence of results was rightfully tested by both authors on the critical velocity, but at a length that was below those we are considering here. As we have shown in the preceding section, the increasing number of modes that play a role in the instability requires, for long ribbons, the use of a larger set of them in the Galerkin approximation.

4.4. On systems tensioned by friction

For other slender systems with axial flow, friction instead of gravity may be the dominant tensioning force. This is the case of horizontal systems such as strips (Watanabe et al., 2002a; Yamaguchi et al., 2000) or cylinders (Ni and Hansen, 1978). The main difference from the case analysed in this paper is that the tensioning force then increases with the flow velocity U, instead of being constant for gravity-induced tension.

Moreover, in the case of axial flow along cantilevered flat structures of smaller aspect ratio, we have pointed out that the physical mechanism of coupling between the motion and the flow differs, because of the change of the plane where the dominant fluctuations of the flow exist. Some comparison may nevertheless be made, as follows. In Watanabe et al. (2002b) the dimensionless mass parameter μ and velocity parameter U_S^* depend on the dimensional length L and velocity U as $U_S^* \sim UL^{3/2}$ and $\mu \sim L^{-1}$. A constant critical velocity would therefore imply that U_S^* varies as $\mu^{-3/2}$. In Watanabe et al. (2002b), Fig. 9, this is not the case for long systems, where $\mu \ll 1$, both for experiments and analytical models. Note that models and experiments in that range differ by about an order of magnitude in critical velocity, but that the variation with μ is parallel. Using these data, it appears that the dimensional critical velocity always decreases with L for such systems. Note that in the intermediate range $0.1 < \mu < 1$ the experimental data are such that U would be almost constant with L. In Yamaguchi et al. (2000) the dimensionless parameter including the flow velocity (denoted by β) varies like $U^{-2}L^{-3}$. In the range of $0.1 < \mu < 1$ experimental and computational results show that $\beta \sim \mu^3$, which implies a constant dimensional velocity when the length is varied. Yet, for longer systems, as pointed out by Yamaguchi (2002), numerical predictions yield an almost constant β, so that the velocity would decrease with length as $U \sim L^{-3/2}$. Therefore, in terms of the effect of length, systems with lower aspect ratio L/B and tensioning induced by friction do not seem to reach a limit state where the critical velocity does not depend on length, contrary to what has been observed here for hanging ribbons.

For cylinders in axial flow, such as towed cyclinders, the fluid forces at the downstream free end play a key role in the mechanism of the instability (Païdoussis, 2003). Depending on the shape of this end, local fluid forces acting there may induce a partially follower force. Triantafyllou and Chryssostomidis (1984) showed that a regime with constant critical velocity for divergence instability may exist for long cylinders, but that its characteristics strongly depend on the proportion of follower and non-follower forces at the end. Recent computations showed that, for very long systems of this type, a behaviour similar to that presented here for ribbons can be predicted, where a flutter instability exists independently of length (de Langre et al., 2005).

5. Conclusion

We have shown experimentally that for hanging ribbon-like structures, i.e. structures of large aspect ratio, the flow velocity that causes flutter does not depend on their length, provided they are long enough. This was observed for a wide range of material and geometrical parameters.

This effect can be understood, at least qualitatively, by considering a simple model of unsteady potential flow along a slender body. Previous uses of this model did not yield the existence of a limit regime for long ribbons, because the number of modes used in the Galerkin approximation was not sufficient to capture the localized flutter at the downstream end. A parallel has been made with the case of hanging fluid-conveying pipes.

For other related systems, such as flags tensioned by friction, existing experiments and models do not show similar behaviour for long systems, which points out the effect of the aspect ratio.

References

Bejan, A., 1982. The meandering fall of paper ribbons. Physics of Fluids 25, 741–742.

Bolotin, V.V., 1963. Non-Conservative Problems of the Theory of Elastic Stability. Pergamon Press, Oxford.

Datta, S.K., Gottenberg, W.G., 1975. Instability of an elastic strip hanging in an air stream. Journal of Applied Mechanics 42, 195–198.

Doaré, O., de Langre, E., 2002. The flow-induced instability of long hanging pipes. European Journal of Mechanics A/Solids 2, 857–867.

Farnell, D.J.J., David, T., Barton, D.C., 2004a. Coupled states of flapping flags. Journal of Fluids and Structures 19, 29–36.

Farnell, D.J.J., David, T., Barton, D.C., 2004b. Numerical simulations of a filament in a flowing soap film. International Journal for Numerical Methods in Fluids 44, 313–330.

Huang, L.X., 1995. Flutter of cantilevered plates in axial flow. Journal of Fluids and Structures 9, 127–147.

de Langre, E., Païdoussis, M.P., Doaré, O., 2005. Flutter of long cantilevered cylinders in axial flow. In: Proceedings of the 20th Canadian Congress of Applied Mechanics, McGill University, Montreal, Canada, 30 May–2 June, pp. 325–326.

Ni, C.C., Hansen, R.J., 1978. An experimental study of the flow-induced motions of a cylinder in axial flow. Journal of Fluids Engineering 100, 389–394.

Païdoussis, M.P., 1966. Dynamics of flexible cylinders in axial flow, Part 2: experiments. Journal of Fluid Mechanics 26, 737–751.

Païdoussis, M.P., 1998. Fluid–Structure Interactions, Slender Structures and Axial Flows, vol. 1. Academic Press, London.

Païdoussis, M.P., 2003. Fluid–Structure Interactions, Slender Structures and Axial Flows, vol. 2. Elsevier, Academic Press, London.

Schouveiler, L., Eloi, C., Le Gal, P., 2004. Flow-induced vibrations of a flexible filament inclined to the flow. In: E. de Langre, F. Axisa (Eds.), Proceedings of the Eighth International Conference on Flow-Induced Vibration, Paris, France, 6–9 July, vol. 1, pp. 185–190.

Timoshenko, S., 1961. Theory of Elastic Stability. McGraw-Hill, New York.

Triantafyllou, G.S., Chryssostomidis, C., 1984. Analytical determination of the buckling speed of towed slender cylindrical beams. ASME Journal of Energy Resources Technology 106, 247–249.

Triantafyllou, G.S., Chryssostomidis, C., 1985. Stability of a string in axial flow. ASME Journal of Energy Resources Technology 107, 421–425.

Watanabe, Y., Suzuki, S., Sugihara, M., Sueoka, Y., 2002a. An experimental study of paper flutter. Journal of Fluids and Structures 16, 529–542.

Watanabe, Y., Isogai, K., Suzuki, S., Sugihara, M., 2002b. A theoretical study of paper flutter. Journal of Fluids and Structures 16, 543–560.

Yadykin, Y., Tenetov, V., Levin, D., 2001. The flow-induced vibration of a flexible strip hanging vertically in a parallel flow. Journal of Fluids and Structures 15, 1167–1185.

Yamaguchi, N., 2002. Private Communication.

Yamaguchi, N., Sekiguchi, T., Yokota, K., Tsujimoti, Y., 2000. Flutter limits and behaviour of a flexible sheet in high-speed flow, Part 2: experimental results and predicted behaviour at low mass ratios. ASME Journal of Fluids Engineering 122, 75–83.

Zhang, J., Childress, S., Libchaber, A., Shelley, M., 2000. Flexible filaments in a flowing soap film as a model for one-dimensional flags in a two-dimensional wind. Nature 408, 835–839.